POLITECNICO DI TORINO
Repository ISTITUZIONALE

Role of cyclic carbonates in enhancing UV-crosslinked PEO-PEC electrolytes for room-temperature lithium metal batteries

Original
Role of cyclic carbonates in enhancing UV-crosslinked PEO-PEC electrolytes for room-temperature lithium metal batteries / Bajaj, R., Darjazi, H., Gastaldi, M., Balducci, L., Elia, G.A., Gerbaldi, C.. - In: JOURNAL OF POWER SOURCES. - ISSN 0378-7753. - ELETTRONICO. - 674:(2026), p. 239777. [10.1016/j.jpowsour.2026.239777]

Availability:
This version is available at: 11583/3008209 since: 2026-03-05T11:43:50Z

Publisher:
Elsevier

Published
DOI:10.1016/j.jpowsour.2026.239777

Terms of use:

This article is made available under terms and conditions as specified in the corresponding bibliographic description in the repository

Publisher copyright

(Article begins on next page)

10 October 2026

Journal of Power Sources 674 (2026) 239777

Contents lists available at ScienceDirect

Journal of Power Sources

journal homepage: www.elsevier.com/locate/jpowsour

Role of cyclic carbonates in enhancing UV-crosslinked PEO-PEC electrolytes for room-temperature lithium metal batteries

Rijul Bajaj [a,b], Hamideh Darjazi [a,b,*], Matteo Gastaldi [a,b], Leonardo Balducci [a,b], Giuseppe Antonio Elia [a,b,**], Claudio Gerbaldi [a,b,***]

[a] Game Lab, Department of Applied Science and Technology (DISAT), Politecnico di Torino, Corso Duca degli Abruzzi 24, 10129, Torino, Italy
[b] National Reference Center for Electrochemical Energy Storage (GISEL) - INSTM, Via G. Giusti 9, 50121, Firenze, Italy

HIGHLIGHTS

- Solvent-free UV-crosslinked PEO–PEC room-temperature solid polymer electrolytes (SPEs).
- Cyclic carbonates unlock high ionic transport and suppress crystallinity.
- Butylene carbonate delivers enhanced Li-metal interfacial stability.
- Dendrite-free Li|SPE|Li cycling sustained for >2300 h at 25 °C.
- Solid-state Li|SPE|LFP cells reach near-theoretical capacity at room temperature.

GRAPHICAL ABSTRACT

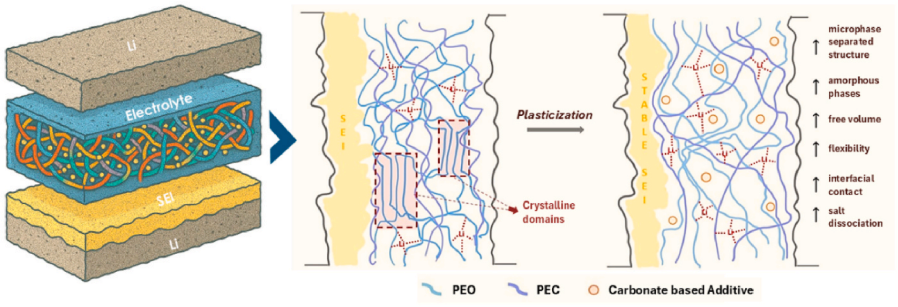

ARTICLE INFO

Keywords:
Lithium battery
Polymer electrolyte
poly(ethylene oxide)
Carbonate
Plasticizer
Crosslinking

ABSTRACT

Future Li-based batteries require electrolytes with high safety, thermal stability, and performance, yet poly (ethylene oxide)-based solid polymer electrolytes (SPEs) remain limited by crystallinity-induced low ionic conductivity and stability at room temperature (RT). In this study, a UV-crosslinked poly(ethylene oxide)-poly (ethylene carbonate) (PEO-PEC) salt-in-polymer matrix is developed through dry melt compounding by a mini twin-screw extruder, followed by hot-pressing and UV-induced photopolymerization(crosslinking). The solvent-free manufacturing is designed to mitigate crystallinity and improve mechanical robustness. Resulting SPEs are further modified with cyclic carbonate plasticizers, namely ethylene carbonate (EC), propylene carbonate (PC), and 1,2-butylene carbonate (BC), to enhance ionic mobility and electrochemical stability, thereby addressing the challenge of fabricating next-generation lithium metal batteries (LMBs) with sufficient ion transport at RT. The influence of these additives, individually and in combination, is investigated through a comprehensive set of electrochemical, thermal, and mechanical characterizations. BC-containing SPEs exhibit reduced glass transition

This article is part of a special issue entitled: MDB 2025 : Progresses and Challenges published in Journal of Power Sources.

* Corresponding author. Game Lab, Department of Applied Science and Technology (DISAT), Politecnico di Torino, Corso Duca degli Abruzzi,24, 10129, Torino, Italy.
** Corresponding author. Game Lab, Department of Applied Science and Technology (DISAT), Politecnico di Torino, Corso Duca degli Abruzzi,24, 10129, Torino, Italy.
*** Corresponding author. Game Lab, Department of Applied Science and Technology (DISAT), Politecnico di Torino, Corso Duca degli Abruzzi,24, 10129, Torino, Italy.
E-mail addresses: hamideh.darjazi@polito.it (H. Darjazi), giuseppe.elia@polito.it (G.A. Elia), claudio.gerbaldi@polito.it (C. Gerbaldi).

https://doi.org/10.1016/j.jpowsour.2026.239777
Received 7 November 2025; Received in revised form 12 February 2026; Accepted 27 February 2026
Available online 5 March 2026
0378-7753/© 2026 The Authors. Published by Elsevier B.V. This is an open access article under the CC BY license (http://creativecommons.org/licenses/by/4.0/).

temperatures and stable compatibility with lithium metal for over 2300 h at a capacity of 0.2 mAh cm^{-2}. In addition, laboratory-scale solid-state Li metal cells with LFP show remarkable performance, delivering almost full practical specific capacity even at RT, despite the presence of immobilized carbonate plasticizers within the crosslinked polymer matrix. This work presents an effective strategy to tailor SPEs for ambient temperature operation through rational additive design, offering insights into the structure-property relationships critical for practical LMB development.

1. Introduction

The drive toward cleaner energy technologies hinges on our ability to develop high-performance, safe, and sustainable energy storage systems. Lithium-ion batteries (LIBs) dominate the energy storage market owing to their high energy density, long cycle life, and efficiency. However, the safety hazards of conventional liquid electrolytes, which are often flammable, volatile, and reactive under thermal and electrochemical stress, have spurred intense research into solid-state electrolytes (SSEs) as safer alternatives. Indeed, next-generation lithium metal batteries (LMBs) must rely on SSEs that, beyond enhancing thermal stability and minimizing leakage risks, also simplify cell design and advance energy storage technologies by enabling the use of high-energy-density electrodes such as lithium metal [1].

Within this class, solid-state polymer electrolytes (SPEs) have attracted considerable attention due to their inherent safety, flexibility, and ease of processing [2–4]. Notably, poly(ethylene oxide) (PEO) has long been the archetypal host polymer for lithium electrolytes [5] because of its excellent solvation ability toward lithium salts and the flexibility of its polymer chains [6]. However, neat PEO suffers from several intrinsic limitations at room temperature (RT). Its high crystallinity reduces amorphous transport pathways, and ionic conductivity remains below 10^{-6} S cm^{-1}. In addition, PEO-based electrolytes typically exhibit a relatively low Li^+ transference number, reflecting significant anion mobility and leading to concentration polarization under current flow [7]. Furthermore, its mechanical strength and dimensional stability are insufficient to suppress lithium dendrite penetration [8], while its electrochemical stability window is limited to below 4.0 V *vs.* Li^+/Li. These drawbacks restrict its compatibility with Li metal and high-voltage cathodes. To address these issues, several approaches have been proposed: i) lowering the polymer's glass transition (T_g) by introducing flexible comonomers or adding plasticizers [9], ii) suppressing crystallinity through copolymerization or blending [10], iii) increasing charge-carrier concentration by optimizing the type and amount of salt [11], iv) incorporating inorganic fillers to create composite electrolytes that promote amorphous structure and provide alternative conduction pathways [12], and v) cross-linking or reinforcing the polymer matrix to enable the use of softer polymers without mechanical failure [13].

Among these strategies, plasticizers, often incorporated as additives (Fig. 1a), modify the microstructure of the polymer matrix, increasing chain mobility and free volume. They effectively reduce the T_g, disrupt crystalline domains, and increase the fraction of amorphous regions, thereby enhancing ion transport pathways [14]. Several families of plasticizers have been investigated to boost the ionic conductivity of PEO-based electrolytes. For instance, succinonitrile (SN) is a plastic-crystalline solvent that, when mixed with PEO, forms a mechanically stabilized gel and achieves ionic conductivity on the order of $\sim 10^{-4}$ S cm^{-1} at RT in fibrous PEO membranes [15,16]. Ionic liquids (e.g. EMI-TFSI, PYR_{14}TFSI, etc.) have also been used as non-volatile plasticizers, simultaneously enhancing ionic conductivity and widening the electrochemical stability windows [17,18]. Cyclic carbonates such as ethylene carbonate (EC) and propylene carbonate (PC), widely used in liquid electrolytes due to their high polarity and ability to form stable interphases, can likewise be incorporated as plasticizers in small amounts to improve RT conductivity [19]. At low concentrations, these aprotic solvents solvate lithium salts and soften the polymer matrix, resulting in gel-like ionic transport while the membrane remains mechanically solid.

EC is an essential component in LIB electrolytes where it is well-known to decompose onto the negative electrode during initial charging to form a robust and stable solid-electrolyte interphase (SEI) layer (Fig. 1b). The formation of such a protective layer enables the use of graphite anodes and is essential for battery's long-term operation, cycle life and safety as it prevents continuous electrolyte decomposition [20]. In addition, EC possesses an exceptionally high dielectric constant ($\varepsilon \approx 90$ at 40 °C) [21,22], which makes it highly effective in dissociating lithium salts into free ions, a key factor for maximizing ionic conductivity in salt-in-polymer systems (Fig. 1c). For instance, adding ~20 wt% EC to a PEO-$LiCF_3SO_3$ electrolyte increases the conductivity at 25 °C to $\sim 3.2 \times 10^{-4}$ S cm^{-1}, compared to only 10^{-6}-10^{-7} S cm^{-1} for the unplasticized system [23]. These values approach those of conventional liquid electrolytes and represent several-thousand-fold improvements over crystalline PEO.

PC, a structural analogue of EC with one additional methyl group on the ring (Fig. 1b), is a low-melting liquid (m.p. ≈ −49 °C) at RT [24]. PC also has a high ε around 64-66, enabling an effective salt dissociation and plasticization [25]. It is widely used in electrochemistry due to its broad liquid range and stability; however, in conventional LIBs, its application with graphite anodes has been limited because PC molecules tend to co-intercalate along with Li^+ ions within the graphene layers, causing expansion of the graphite structure and detrimental exfoliation (Fig. 1c) [70,26]. Notably, PC is more resistant to reduction than EC, though it forms a poorer SEI on graphite due to co-intercalation and high solubility of its reduction products [27,28], and in polymer electrolytes, it has been shown to greatly increase ionic conductivity [25]. For example, a mixed EC/PC plasticizer in PEO yielded $\sim 4 \times 10^{-4}$ S cm^{-1} at

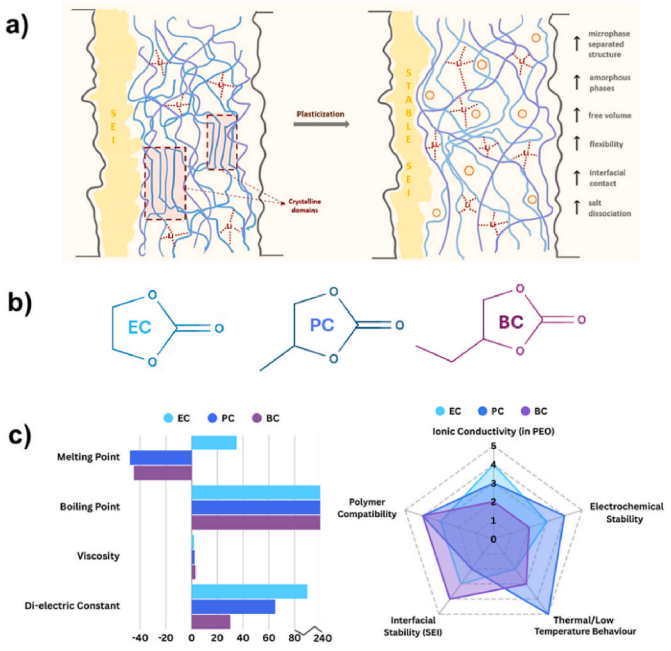

Fig. 1. a) Schematic representation of the effect of plasticizers on SPEs; b) chemical structures of EC, PC, and BC, and c) related theoretical properties and performance indicators.

25 °C [39]. The key advantages of PC are its liquidity at RT and its ability to suppress crystallization in the polymer matrix, ensuring that polymer electrolytes remain flexible and amorphous even at low temperatures [30].

1,2-Butylene carbonate (BC) is a less-studied cyclic carbonate in battery applications. Structurally, BC differs from PC by an extra –CH_2– substituent (Fig. 1b). It is a liquid at RT (m.p. ≈ −50 °C) [31] and retains a high ε (>50) [32], providing strong salt-solvating capability (Fig. 1c) [33]. Hence, BC offers a more organized solvent structure and bulkier ethyl groups that effectively separate polymer chains, increasing the free volume and facilitating "hopping" mechanisms. Importantly, the bulkier substituents enhance oxidative stability compared with EC and PC, enabling BC to withstand higher voltages before oxidation [29,34]. Despite these promising characteristics, BC has not been widely employed in polymer electrolytes to date, and its potential as a plasticizer remains underexplored. A comparative summary of the key physicochemical and electrochemical properties of EC, PC, and BC is provided in Table S1.

Beyond plasticization, structural modification strategies such as UV-induced crosslinking (UV-curing) and polymer blending have also proven highly effective [13]. UV-induced polymerisation is especially attractive, as it can generate crosslinked polymer networks within minutes, allowing for reduced polymer crystallinity and controlled network structure, concurrently enhancing ionic conductivity under mild conditions and mechanical properties like strength and flexibility [13,35]. Polymer blending, on the other hand, offers a practical route to reinforce structural stability while improving electrochemical performance [36,37]. One promising candidate is poly(ethylene carbonate) (PEC), a polycarbonate-based polymer with a high ε, reduced crystallinity, and better oxidative stability compared to PEO [38,39]. PEC possesses a more flexible backbone, and its carbonate groups interact favourably with lithium ions [48,40]. However, despite these advantages, pure PEC electrolytes are too soft and dimensionally unstable for practical rechargeable cell operation [2,38,39]. To overcome this limitation, in our previous work, we developed PEO–PEC SPEs via a solvent-free extrusion process followed by UV-curing [38]. The optimized blends exhibited significantly enhanced ionic conductivity below PEO m.p., along with improved tensile strength, illustrating the effectiveness of polymer blending. Moreover, the solvent-free, scalable extrusion approach well couples with UV-curing, aligning with the requirements of high-throughput industrial solid-state battery manufacturing [41].

In this work, we conduct a comprehensive study of UV-cured PEO–PEC-based SPEs modified with controlled fractions of cyclic carbonate plasticizers (EC, PC, and BC) to enhance the RT performance of SSLMBs. The UV-curing process yields mechanically robust membranes while immobilizing the non-volatile additives, thereby preventing leakage despite the presence of liquid-like plasticizers. Incorporation of cyclic carbonates into the PEO–PEC network is designed to: i) increase the amorphous fraction and lower the T_g, thereby enhancing ionic conductivity at 25 °C, ii) provide a high-dielectric environment that promotes lithium salt dissociation and increases charge-carrier density, and iii) improve interfacial stability against the lithium metal anode by facilitating the formation of a stable SEI [20,42]. To validate these hypotheses, we systematically evaluate the individual and combined effects of cyclic carbonates on ionic conductivity, mechanical integrity, and electrode compatibility. Our results demonstrate that the tailored incorporation of cyclic carbonates markedly improves the electrochemical performance of UV-cured PEO–PEC-based electrolytes at 25 °C, advancing them toward practical application in SSLMBs.

2. Experimental

2.1. Materials and reagents

Poly(ethylene oxide) (PEO, molecular weight = 4 × 10^5 g mol^{-1}, CAS No. 25322-68-3) was purchased from Merck, while poly(ethylene carbonate) (PEC, molecular weight = 2.43 × 10^5 g mol^{-1}, CAS No. 25608-11-1) was obtained from Specific Polymers (France). The lithium salt bis(trifluoromethanesulfonyl)imide (LiTFSI, battery grade, CAS No. 90076-65-6) and the photoinitiator 4,4′-difluorobenzophenone (DFBP, 99%, CAS No. 345-92-6) were supplied by Merck. All polymers were thoroughly dried under vacuum at 60 °C for 72 h prior to use. LiTFSI was subjected to a three-step drying process: 24 h under vacuum at RT, followed by 48 h at 70 °C, and a final 2 h at 110 °C. All drying procedures were performed in a Buchi B-585 glass drying oven (Switzerland). Anhydrous N-methyl-2-pyrrolidone (NMP, CAS No. 872-50-4) was acquired from Merck and used as received. Conductive carbon black (C65, Imerys) and poly(vinylidene fluoride) (PVdF, Solef 6020, Solvay) were used without further purification. Lithium iron phosphate ($LiFePO_4$, LFP) cathode powder was provided by BASF. Battery-grade ethylene carbonate (EC, CAS No. 96-49-1) and propylene carbonate (PC, CAS No. 108-32-7) were procured from Solvionic and used as received. 4-Ethyl-1,3-dioxolan-2-one (1,2-butylene carbonate, BC, 99%, CAS No. 4437-88-8) was purchased from BLDpharm and used without further purification.

2.2. Preparation of crosslinked solid polymer electrolytes (SPE)

All electrolyte formulations and processing steps were conducted in an argon-filled glovebox (O_2 and H_2O < 0.1 ppm, M-Braun) unless otherwise stated. SPEs were prepared via a solvent-free melt compounding method using a mini twin-screw extruder (Haake MiniLab II, Thermo Scientific). The extrusion procedure followed a previously optimized and reported protocol [38]. Initially, the appropriate amounts of PEO and PEC (maintaining a 1:1 wt ratio) were weighed inside the glovebox and divided into two portions. The first portion of the PEO/-PEC blend was introduced into the pre-heated extruder, followed by the addition of LiTFSI (maintaining a fixed [EO]:[Li^+] molar ratio of 20:1) and 4,4′-difluorobenzophenone as the photoinitiator (for UV-curable formulations). Subsequently, the remaining PEO/PEC portion was added. The entire mixture was compounded under a continuous nitrogen purge at 120 °C and 120 rpm for 10 min to ensure complete homogenization and salt solubilization. The resulting homogeneous blends were extruded as filaments, immediately transferred under vacuum to remove any residual volatiles, and then stored in the glovebox. Cyclic carbonate additives (EC, PC, BC, or their 1:1 wt mixtures) were encompassed into the polymer blend at 20 wt% with respect to the total polymer content (PEO + PEC). The additives were blended into the solid electrolyte matrix using a mortar and pestle inside the glovebox until uniform dough-like mixtures were obtained. These were then hot-pressed under inert atmosphere at 70 °C and 15 bar using a pre-heated hydraulic press (after pre-conditioning the material at 70 °C for 10 min) to yield self-standing electrolyte membranes of ~100 μm thickness and ~10 cm diameter. To obtain crosslinked electrolyte films, the same hot-pressing process was applied, directly followed by UV-induced photopolymerization (crosslinking) using a DMAX ECE 5000 UV flood lamp (output: 40 mW cm^{-2}). Samples were irradiated for 3 min on each side at ~70 °C. After UV-curing, all SPE membranes were subjected to an additional drying step at 40 °C under vacuum for 12 h (Buchi B-585 oven) to remove any trace moisture or volatile impurities, then stored in the glovebox until further use. All formulations maintained a fixed [EO]:[Li^+] molar ratio of 20:1, a value previously reported as optimal for balancing ionic conductivity and film-forming properties [43]. The PEO:PEC weight ratio was also fixed at 1:1, which has been shown to yield membranes with good mechanical integrity and suppressed crystallinity [38]. The final membranes appeared as quasi-transparent, homogeneous, and elastic films suitable for structural and electrochemical tests (Fig. 2).

a)

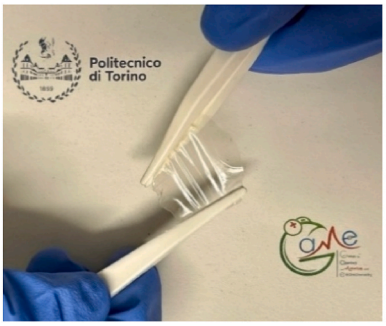

b)

Samples	Plasticizer (20% by weight of polymer)	Acronyms
PEO-PEC (1:1) + LiTFSI + DFBP	Ethylene Carbonate	EC
	Propylene Carbonate	PC
	1,2-butylene carbonate	BC
	Ethylene Carbonate : Propylene Carbonate (1 : 1)	EC-PC
	Ethylene Carbonate : 1,2-butylene Carbonate (1 : 1)	EC-BC
	Propylene Carbonate : 1,2-butylene Carbonate (1 : 1)	PC-BC
	Ethylene Carbonate : Propylene Carbonate : 1,2-butylene Carbonate (1 : 1 : 1)	EC-PC-BC

Fig. 2. a) Self-standing, mechanically stable, and flexible PEO-PEC-carbonate-based SPE; b) corresponding sample acronyms and formulations as discussed in this study.

2.3. Characterisation techniques

To comprehensively evaluate the physicochemical and electrochemical properties of the prepared SPEs, a series of characterization techniques was employed as described below.

The ionic conductivity (σ) of the SPE membranes was determined using electrochemical impedance spectroscopy (EIS), performed on a VMP-3 potentiostat/galvanostat (Bio-Logic, France). Circular membrane samples (16 mm diameter, ~100 μm thickness) were sandwiched between two stainless steel (SS) blocking electrodes, forming an SS||SPE||SS cell configuration, and mounted in EL-Cell standard test cells (EL-CELL, Germany). The exact thickness of each membrane was measured both before and after testing using a precision micrometer (Mitutoyo). EIS measurements were conducted over a frequency range of 0.1 Hz to 1 MHz with an applied AC perturbation of 20 mV. Measurements were performed across a temperature range of 0 to 80 °C in 10 °C increments using a temperature-controlled climatic chamber (MK 53 E2, BINDER, Germany). To ensure thermal equilibrium at each temperature point, cells were held for 100 min prior to measurement. Nyquist plots were analysed using EC-Lab software, and the bulk resistance (R) was extracted from the high-frequency intercept. Ionic conductivity was then calculated using the relation:

$$\sigma = D/AR$$

where D is the membrane thickness (cm), A is the electrode area (cm^2), and R is the resistance (Ω).

The electrochemical stability window (ESW) of the SPEs was assessed by linear sweep voltammetry (LSV). The tests were conducted at RT using a Li||SPE||carbon-coated aluminium (CC-Al) cell configuration, where Li metal (Albemarle) served as the counter/reference electrode and CC-Al as the working electrode. The CC-Al electrodes were prepared by casting a slurry composed of conductive carbon black (C65, 80 wt%) and PVdF binder (20 wt%) in NMP onto aluminium foil. The coated films were dried at RT overnight, punched into disks, and then vacuum dried at 120 °C for 24 h to eliminate residual solvent and moisture. LSV measurements were conducted at a scan rate of 1 mV s^{-1} from open circuit voltage (OCV) up to 6.0 V vs. Li^+/Li. The onset of oxidative decomposition was defined as the potential at which the current density exceeded 5 μA cm^{-2}.

The lithium-ion transference number (t_{Li}^+) was determined using a combination of direct current (DC) polarization and alternating current (AC) impedance methods. The AC impedance spectra before and after polarization were obtained via EIS [44]. The transference number was calculated using the following equation:

$$t_{Li^+} = \frac{I_s(\Delta V - I_o R_o)}{I_o(\Delta V - I_s R_s)}$$

where R_0 is the impedance resistance before polarization. R_s is the impedance after DC polarization. I_0 is the initial current, I_s is the final current after polarization, and represents the applied polarization voltage (30 mV).

To evaluate the electrochemical cycling stability and compatibility of the SPEs with lithium metal, galvanostatic cycling with potential limitation (GCPL) tests were carried out at RT using symmetric Li||SPE||Li cells. The cells were assembled under inert atmosphere with 12 mm lithium electrodes and 16 mm electrolyte discs in CR2032 coin cells. Cycling was performed at current densities of 0.025 and 0.05 mA cm^{-2} with a fixed plated/stripped areal capacity per half/cycle of 0.2 mAh cm^{-2}. These tests enabled assessment of interface stability and polarization behaviour under varying current loads. For the most promising electrolyte composition, lithium plating/stripping stability was further investigated under prolonged cycling at 0.025 mA cm^{-2} (areal capacity: 0.2 mAh cm^{-2}) at RT to evaluate dendrite suppression and interface longevity. Based on the ionic conductivity results, additional measurements were conducted at 50 °C under higher current density of 0.05 mA cm^{-2} to further evaluate cycling performance.

Thermal stability was evaluated via thermogravimetric analysis (TGA) using a Netzsch TG 209 F3 instrument. Measurements were performed under a nitrogen atmosphere over the temperature range 25-800 °C at a heating rate of 10 °C min^{-1}. Differential scanning calorimetry (DSC) was conducted using a Netzsch DSC 214 Polyma system to determine the glass transition temperature (T_g). The DSC scans were recorded from −80 to 90 °C at a heating rate of 20 °C min^{-1} under nitrogen flow (40 mL min^{-1}).

The viscoelastic and thermo-mechanical properties of the membranes were investigated using dynamic mechanical thermal analysis (DMTA) on a Q800 instrument (TA Instruments). Measurements were conducted using rectangular bar specimens obtained from the SPE membranes. A fixed oscillation frequency of 1 Hz was applied, and temperature was ramped from −70 to 60 °C at a rate of 3 °C min^{-1}. The storage modulus (E′), loss modulus (E″), and relaxation temperature (identified as the peak in the E″ curve) were recorded to assess the mechanical robustness and thermal transitions relevant for practical battery operation.

To assess the electrochemical performance of the optimized SPE in a practical Li-based cell configuration, laboratory-scale SSLMB cells were assembled in a Li||SPE||LFP configuration housed in an EL-Cell Std test cell (EL-CELL, Germany). The galvanostatic cycling tests were conducted at both RT and 50 °C to assess rate capability under realistic operating conditions. The charge/discharge rates were sequentially varied from C/40 to C/5 (i.e., C/40, C/20, C/10, and C/5), with each rate applied for five full cycles. The protocol concluded with a return to C/20 to evaluate capacity recovery. A 1C rate corresponds to a current density of 170 mA g^{-1}, calculated based on the mass of the LFP active material. For the fabrication of the LFP cathode, PVdF was first dissolved

in NMP under continuous stirring. A mixture consisting of the active material and conductive carbon (Super C65) was prepared separately by thorough mixing and grinding. This mixture was then incorporated into the PVDF/NMP solution to obtain a slurry with a mass ratio of active material:Super C65:PVDF = 75:15:10. A Thinky mixer was employed to ensure complete homogenization of the slurry. The resulting slurry was cast onto aluminium foil using a doctor blade with a gap of 150 μm. The coated films were dried at 70 °C for 2 h, followed by room temperature drying. Subsequently, the electrodes were calendered, cut into shape, and subjected to vacuum drying overnight at 120 °C. The active material mass loading was in the range of 2.5 mg cm^{-2}. For room-temperature electrochemical testing vs. Li metal, the polymer membrane was hot-pressed onto the surface of the cathode to ensure good interfacial contact. NMC622 cathodes were prepared analogously using a NMC622: Super C65:PVDF mass ratio of 80:10:10, with an active material loading of ~3.2 mg cm^{-2}; 1C was defined as 170 mA g^{-1}.

3. Results and discussion

3.1. Electrical and electrochemical characterization

The ionic conductivity (σ) of the prepared SPEs was evaluated by EIS at various temperatures (Fig. 3a). All samples display a change in slope around ~40 °C in the Arrhenius plots, corresponding to the melting of crystalline regions in the PEO-based matrix and a transition to a predominantly amorphous phase [45]. However, due to the combined effects of UV curing, extrusion processing, lithium salt coordination, and the incorporation of plasticizers, this thermal transition is significantly attenuated compared to that of standard semi-crystalline PEO. The gradual amorphization enhances polymer chain mobility, leading to a steeper rise in σ as ion transport proceeds in a more rubbery-amorphous environment [46,47]. Such behaviour is beneficial, as moderate heating (40-60 °C) activates significantly higher ionic conductivity, thereby expanding the practical operating temperature range of the electrolyte. At RT, all SPEs exhibit ionic conductivities on the order of ~10^{-5} S cm^{-1}, increasing to ~10^{-4} S cm^{-1} at 80 °C, values comparable to additive-free SPE [48]. In particular, the EC-containing SPE exhibits a higher σ beyond ~40 °C compared to PC or BC alone, owing to its phase behaviour and high dielectric constant [49]. Once melted, EC acts as a highly effective plasticizer, enhancing polymer segmental motion and lithium salt dissociation, thereby boosting σ.

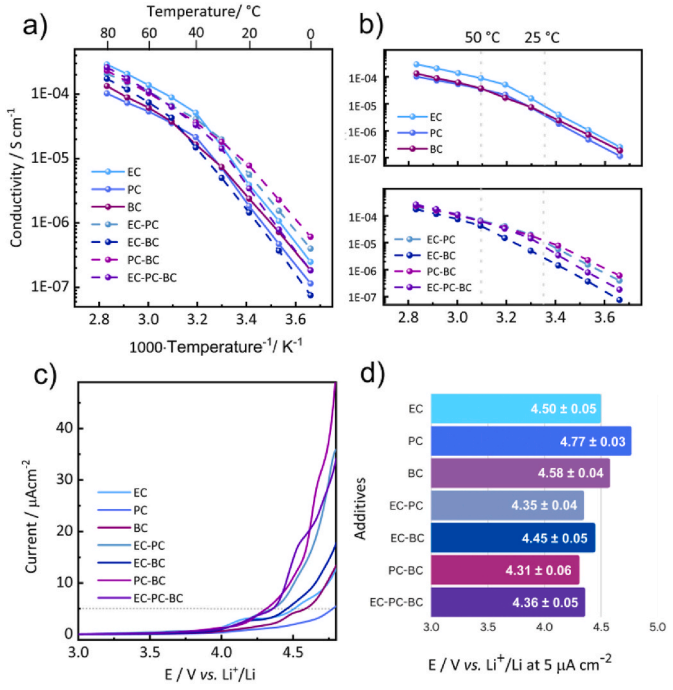

Fig. 3. (a) Arrhenius plots of ionic conductivity vs. inverse temperature; (b) magnified view of segregated Arrhenius plots from a); (c) linear: sweep voltammetry (LSV) curves at RT, and (d) bar plot summarizing ESW values derived from LSV data, of various SPEs under study.

Fig. 3b shows the LSV curves used to determine the ESW of the SPEs at RT. All samples exhibit broad oxidative stability, with onset of measurable oxidation currents (threshold ~5 μA cm^{-2}) beyond ~4.3 V *vs.* Li^+/Li. Among the single-additive systems, the PC-containing SPE demonstrates the highest stability, with no significant oxidation until about 4.77 V *vs.* Li^+/Li, followed by BC (4.58 V) and EC (~4.5 V). By contrast, the mixed additives SPEs (binary and ternary blends) show slightly lower stability, with current onset in the range of 4.3-4.4 V. This minor reduction could be due to the least stable component in the mixture dominating the overall onset of oxidation, or from synergistic solvent interactions between additives that modestly lower the stability threshold. Nevertheless, all SPE membranes still exceed ~4.3 V *vs.* Li^+/Li before appreciable oxidation, indicating that these electrolytes can be used with standard cathodes without oxidative decomposition.

The Li^+ transference number measured by the Bruce-Vincent-Evans method is ~0.20 at room temperature (Fig. S1), consistent with typical PEO-based polymer electrolytes [7], indicating that the performance improvements observed here primarily originate from enhanced segmental dynamics and reduced crystallinity rather than selective Li^+ transport.

To evaluate the interfacial stability of the SPEs against lithium metal, galvanostatic Li plating/stripping experiments were carried out in symmetric Li||SPE||Li cells at RT (Fig. S2), using current densities of 0.025 and 0.05 mA cm^{-2} with a fixed plated/stripped areal capacity of 0.2 mAh cm^{-2} per half-cycle. All SPEs exhibit stable Li plating/stripping cycling at 0.025 mA cm^{-2}, with minimal overpotentials in the order of 0.1 V for the single-additive SPEs and slightly higher for the binary/ternary ones, and no signs of dendritic growth or instability, reflecting their ability to sustain lithium cycling at low current. When the current increases to 0.05 mA cm^{-2}, only the single-additive BC and PC systems sustain stable cycling. In both cases, the cell voltages gradually rise to a maximum overpotential of ~0.3 V, but remain relatively steady without abrupt fluctuations, indicating a robust Li/SPE interface. In contrast, binary and ternary blend SPEs show erratic behaviour, with sudden voltage spikes and asymmetric plating/stripping profiles. These irregularities suggest uneven lithium deposition and the onset of transient "soft short-circuits", likely caused by the formation of nascent dendrites, confined dendritic Li penetration through the polymer electrolyte or localized high-resistance regions at the interface [50–52]. The absence of such behaviour in single-additive BC-based and PC-based systems promotes a more stable and uniform interface, whereas binary/tertiary blends might introduce heterogeneity in ionic conductivity or mechanical properties, leading to uneven current distribution and unstable Li plating. Based on these preliminary findings, BC-based and PC-based SPEs stand out as the most promising candidates, warranting further detailed investigations to comprehensively assess their physicochemical and electrochemical characteristics.

Given their superior performance, the single-additive BC and PC SPEs were further evaluated via extended galvanostatic plating/stripping cycling at 0.025 mA cm^{-2} in Li||SPE||Li symmetric with a fixed plated/stripped capacity of 0.2 mAh cm^{-2} per half-cycle at 25 °C (Fig. 4) to evaluate long-term lithium metal compatibility. Under identical testing conditions, both electrolytes demonstrate stable long-term operation, sustaining for ~2300 h of plating/stripping without short-circuiting. The BC-based SPE cell (Fig. 4a) shows initial steady-state overpotential of around 0.15 V and remains nearly constant for the first ~1600 h, indicating the formation of a stable SEI and optimal Li/SPE interfacial contact, implying highly reversible charge transfer at the interface. After ~1600 h, a gradual rise in overpotential is observed, eventually reaching ~0.25 V by the end of the test. This trend is

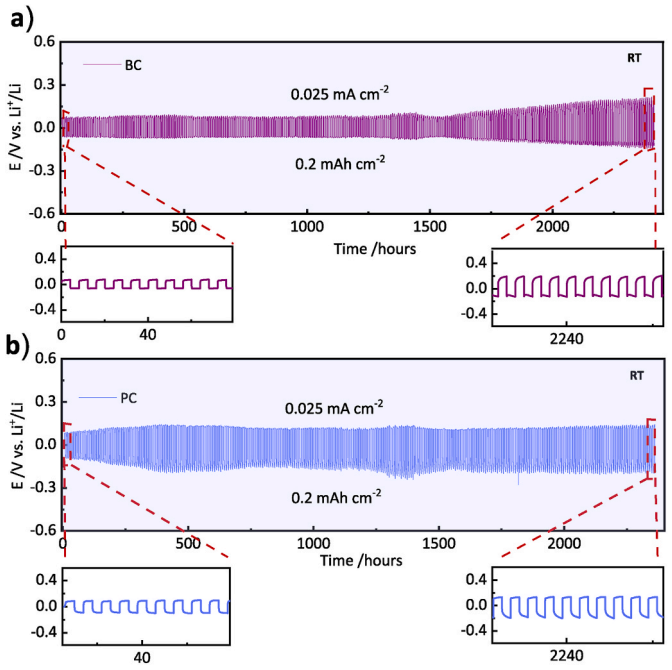

Fig. 4. Long-term plating/stripping galvanostatic cycling of Li symmetric cells using (a) BC-based and (b) PC-based SPEs at a current density of 0.025 mA cm^{-2} at RT.

consistent with progressive interfacial resistance buildup (areal specific resistance increased from ~6 × 10^3 to ~11 × 10^3 Ω cm^2) likely due to the continuous growth of a resistive solid–electrolyte interphase (SEI) and/or reduced wetting between Li and the polymer electrolyte. In contrast, the PC-based SPE (Fig. 4b) shows a slightly higher initial overpotential (~0.20 V) with more fluctuations over time, suggesting a less uniform Li deposition or slightly less stable interphase.

Based on the ionic conductivity results and to complement the SSLMB cell testing, the BC-based SPE was characterised by additional measurements at 50 °C under increasingly higher current densities of 0.025, 0.05, 0.1 mA cm^{-2} (Fig. S3). The cell exhibits stable lithium plating/stripping with low overpotential values at both 0.025 and 0.05 mA cm^{-2} (Fig. S3a). To further evaluate its robustness, prolonged cycling was carried out at 0.05 mA cm^{-2} (Fig. S3b), showing stable performance with limited overpotential increase for over 320 h. The overpotential shows only minor changes over the test, indicating a stable lithium plating/stripping interface and suppression/limitation of dendritic growth under the applied low current density conditions, which is remarkable for a SPE cycled at RT.

3.2. Thermomechanical characterization

Thermal and mechanical characterization of BC-based and PC-based SPEs were conducted to evaluate stability and structural integrity (Fig. 5). Thermal stability was evaluated by thermogravimetric analysis (TGA) under inert atmosphere to determine the upper temperature threshold before degradation (Fig. 5a,d). The TGA curves of both SPEs reveal three distinguishable weight-loss steps. The initial minor loss above 100 °C is attributed to the release of residual volatiles, predominantly absorbed moisture, associated with the hygroscopic LiTFSI salt and the polar polymer host, and is not expected to influence

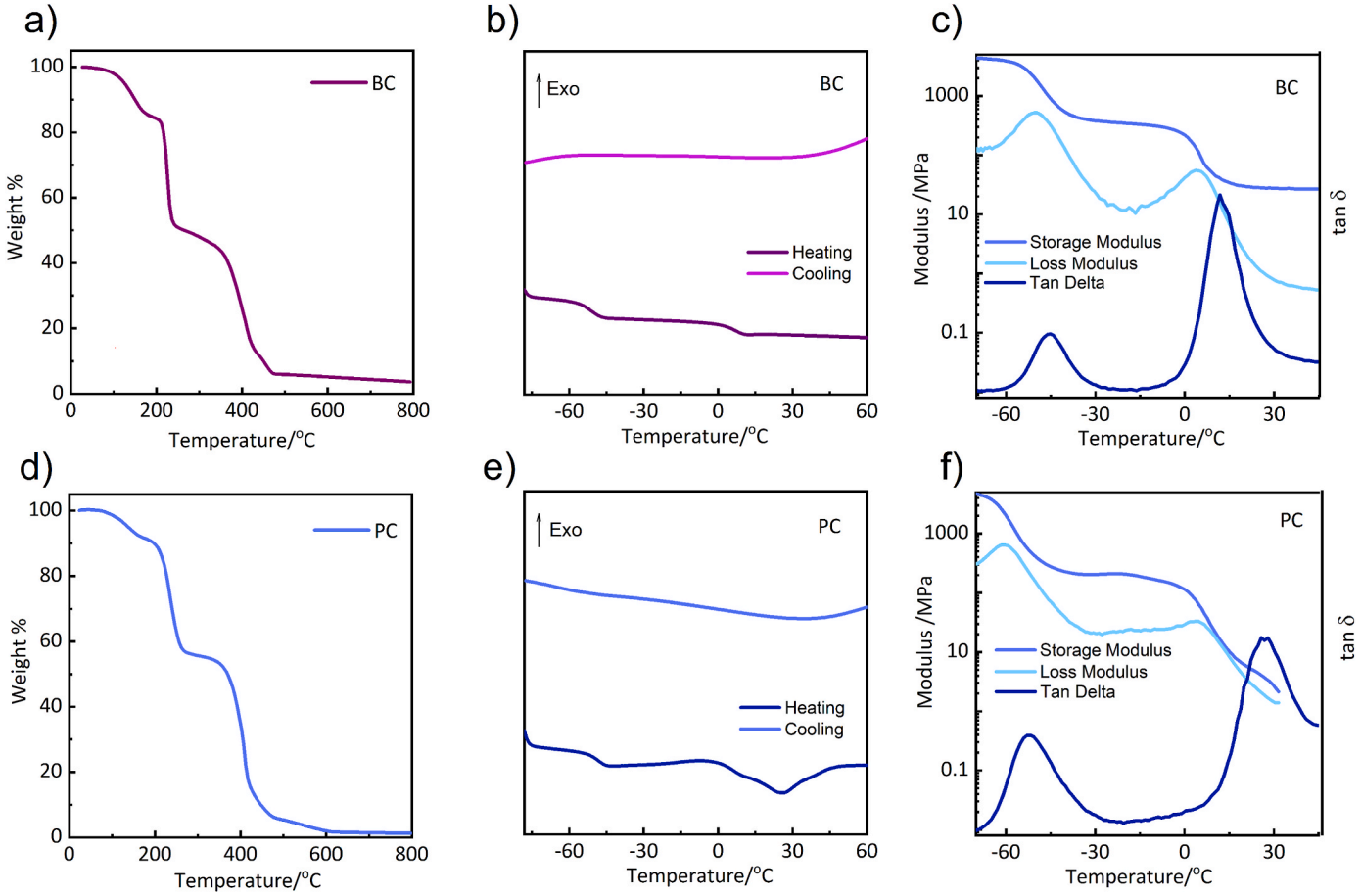

Fig. 5. Comparative thermal and mechanical analyses of BC-based and PC-based SPEs: (a,d) TGA profiles, (b,e) DSC curves, and (c,f) DMA curves.

electrochemical performance, as it occurs well above the standard battery operating temperature and no progressive degradation or interfacial instability was observed during long-term cycling [53–57]. Importantly, this event occurs below the intrinsic degradation onset of the polymers (>120 °C), indicating that the extrusion process (~120 °C) did not induce chemical degradation of the matrix, consistent with prior reports on PEO/polycarbonate systems [38].

The second, more pronounced mass-loss step initiates slightly above 200 °C, corresponding to the thermal decomposition of the aliphatic polycarbonate phase and the volatilization of any organic carbonate additive. In particular, PEC is known to thermally degrade at around 218 °C in the absence of salt, while the incorporation of LiTFSI further reduces its stability, triggering decomposition near ~200 °C [58]. This drop likely corresponds to cleavage of the carbonate polymer chains in conjunction with evaporation of residual plasticizing carbonates. The final major weight-loss step occurs in the 350-420 °C range, typically attributable to the decomposition of the PEO polymer backbone and its complexes with LiTFSI under non-oxidative conditions. While pristine high-molecular-weight PEO typically begins to decompose around ~370 °C, salt-doped membranes exhibit a two-step pathway: an initial chain-scission process (380–390 °C), followed by breakdown of lithium-ethylene oxide complexes up to ~430 °C [59]. This dual-stage behaviour is a well-recognized salt-catalysed phenomenon. By ~450 °C, the decomposition is essentially complete, leaving only inorganic residues derived from LiTFSI decomposition.

Differential scanning calorimetry (DSC) was performed to assess the thermal transitions and crystallinity of the SPEs (Fig. 5b,e). Since Li^+ ion transport in PEO occurs mainly in the amorphous phase, reducing crystallinity is essential for high ionic conductivity [60]. Pure PEO is typically semi-crystalline ($T_m \approx 65$ °C, ~70% crystallinity) [61], but in both BC- and PC-based SPEs, no clear melting or crystallization peaks appear, confirming a largely amorphous character. UV-induced crosslinking effectively suppresses PEO recrystallization [62], and the addition of PEC further disrupts PEO crystallite formation [63]. Both membranes display two T_g transitions, near −50 °C (PEO-rich phase) and ~10 °C (PEC-rich phase), indicating phase separation while retaining individual dynamic behaviours [48]. Compared to UV-cured PEO–PEC systems without plasticizers, both T_g values are depressed by ~10 °C due to BC or PC, which act as plasticizers by increasing free volume and chain mobility [64]. Since ionic transport is strongly coupled to polymer dynamics, this enhanced flexibility favours Li^+ mobility at low (below PEO m.p.) temperature [65]. The BC-based membrane remains predominantly amorphous, while the PC-based membrane shows a minor endothermic feature near 25 °C. This may arise from partial recrystallization of PEO microdomains during DSC cooling, or from localized ordering induced by additive-polymer interactions. A more detailed explanation is the well-known Li^+-PC complexation behaviour in LiTFSI-based electrolytes [66]. Studies using femtosecond vibrational spectroscopy and computational analysis have demonstrated that in high-concentration PC-Li^+ systems, PC tends to form solvent-separated ion clusters with defined coordination geometries, notably $Li(PC)_4^+$ at low salt concentrations, and primarily $Li(PC)_2^+$ plus ion-anion contact species at higher salt concentrations [67,68]. These Li-PC solvate complexes can adopt clathrate-like, cage molecular arrangements, which exhibit a melting or dissociation peak. When incorporated into a polymer matrix, even a crosslinked one, such complexes can retain transient order that registers as a low intensity melting endotherm around RT [66,67].

Dynamic mechanical analysis (DMA) clearly evidences T_g reductions and phase-separated morphology in the SPEs (Fig. 5c,f). The loss modulus (E″) curves exhibit two distinct α-relaxation peaks for both SPEs, corresponding to the glass transitions of the individual PEO- and PEC-rich domains. The first transition, observed at ~ -50 °C, corresponds to the T_g of the PEO-rich phase, while the second peak at ~10 °C is assigned to the T_g of the PEC-rich domain. These temperatures are ~10 °C lower than those reported for unplasticized PEO-PEC blends with LiTFSI (i.e., −30 °C and +20 °C, respectively [48]), confirming the plasticizer-induced softening of both phases. Notably, Li^+ ion coordination with PEO raises the T_g by acting as temporary crosslinking points between PEO chains (it reduces polymer chain mobility, in turn increasing local rigidity of the material) [69]. However, the introduction of cyclic carbonates counteracts this salt-induced stiffening, bringing the T_g closer to that of uncoordinated PEO. This suggests that BC and PC may interfere with the Li^+-PEO coordination, either by directly solvating Li^+ or by modifying the local polymer environment to facilitate motion. In this way, the additives enhance polymer dynamics, even in the presence of coordinating salts.

The double-T_g behaviour observed by DSC and DMA confirms that the UV-cured SPEs are two-phase amorphous blends. This phase separation is beneficial: the PEO-rich phase supports ion transport, while the PEC-rich phase (also softened by plasticizers) provides mechanical stability and thermal resistance. Lowered T_gs widen the temperature window where the polymer chain remains flexible and mobile, enhancing Li^+ conductivity and mechanical compliance at room temperature.

3.3. Electrochemical testing in solid-state LMB cells

The electrochemical applicability of the BC-based SPE was evaluated in laboratory-scale Li-metal cells with composite LFP-based cathodes in the Li||SPE||LFP configuration (Fig. 6). Testing was performed at both 25 and 50 °C, with the latter temperature chosen to promote enhanced segmental motion in the polymer matrix. Rate capability measurements were carried out under galvanostatic cycling at increasingly higher current rates from C/40 to C/5, followed by a return to C/20 for evaluating reversible capacity recovery.

At 25 °C, the specific capacities are approximately 152, 150, and 132, respectively, up to C/10 rate (Fig. 6a), demonstrating remarkable RT performance as well as efficient Li^+ transport at low C-rate and stable cycling under increasing current stress. The drop in the specific capacity to 100 mAh g^{-1} at C/5 suggests a rather resistive passive layer, being not fully effective in allowing excellent cycling at higher rates, thus leading to lower cell performance at high current regimes. The initial Coulombic efficiency (ICE) is ~94%; however, at C/10, the efficiency declines before stabilizing in subsequent cycles and reaching >99% at higher C/5

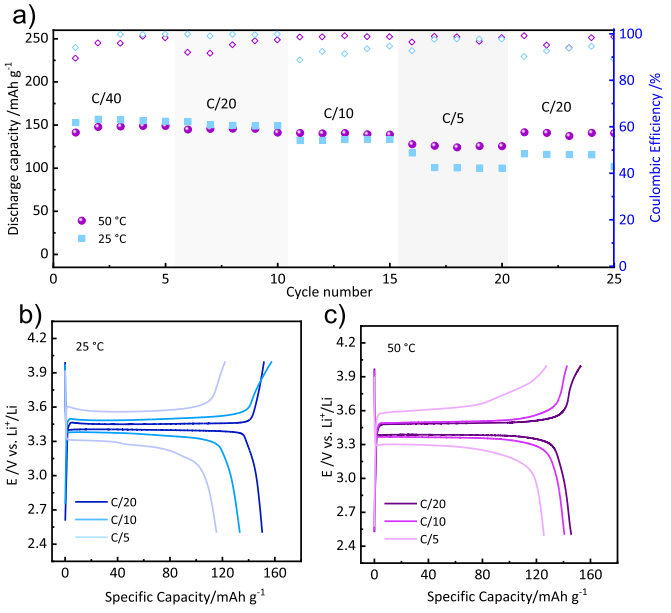

Fig. 6. Galvanostatic cycling behaviour of the BC-based SPE in Li||SPE||LFP at 25 and 50 °C: a) rate capability test upon discharge with related Coulombic efficiency and (b,c) the corresponding voltage profile curves of charge and discharge.

rate. When tested at 50 °C, the cell delivers improved performance, achieving a capacity of ~126 mAh g^{-1} at C/5 (Fig. 6a). As illustrated in Fig. 6b and c, profiles show the typical features of lithium insertion/extraction in the LFP active material with flat plateaus; voltage polarization remains low across tested current densities, with only slight increase at elevated C/5 rate, highlighting the excellent reversible cycling performance of the SPE. These results indicate that interfacial resistance between the SPE and LFP electrode remains stable during operation and that Li^+ transport pathways are well maintained throughout cycling.

To evaluate compatibility with higher-voltage cathodes, preliminary tests were performed using NMC622 cells cycled at 50 °C across different C-rates. The charge/discharge profiles (Fig. S4) display the characteristic voltage behaviour of the NMC cathode and deliver good capacity at C/40. However, increasing the current leads to a noticeable capacity drop, indicating that further optimization of the cathode–electrolyte interface and solid-state transport kinetics is required to fully exploit the wide electrochemical stability window of the SPE in high-voltage systems.

In summary, the BC-based SPE demonstrates to be a promising candidate for safe, high-performing SSLMBs conceived for RT operation, paired with a LFP cathode. The decreased performance at increased current regimes can be linked with the expected increased polarization, requiring specific additives and/or additional electrode manufacturing (catholyte preparation) optimization to be mitigated to achieve stable long-term operation at ambient conditions, which is out of the scope of the present work.

A comparison with previously reported PEO-based SPEs with plasticizers, focusing on processing strategy, glass transition temperature, room-temperature ionic conductivity, interfacial stability, and electrochemical performance, is summarized in Table S2, underscoring the key advances and impact of the present work.

4. Conclusions

In this study, crosslinked PEO–PEC SPEs were successfully developed through fully solvent-free extrusion/UV-induced polymerisation procedure and systematically modified through the incorporation of cyclic carbonate plasticizers, namely EC, PC, and BC, and binary/ternary mixtures thereof. The tailored introduction of these cyclic carbonates was found to markedly enhance the electrochemical properties of the electrolytes at 25 °C, rendering them highly promising for practical SSLMB applications. The improvements arise from the unique physicochemical role of cyclic carbonates in the polymer matrix, which concurrently increased the amorphous content, lowered the T_g, and generated a high-dielectric environment that favoured lithium salt dissociation and charge carrier availability. Furthermore, their presence contributed to improved interfacial stability against lithium metal, facilitating the development of a stable and robust SEI.

Among the investigated systems, the single-additive BC- and PC-based SPEs demonstrated the highest electrochemical performance. Symmetric Li||Li cells assembled with these electrolytes showed stable plating/stripping for ~2300 h at 0.025 mA cm^{-2} with a fixed plated/stripped capacity of 0.2 mAh cm^{-2} per half-cycle, without evidence of short-circuiting. Notably, the BC-based SPE displayed the most stable interfacial behaviour, as reflected by a steady-state overpotential of approximately 0.15 V maintained over ~1600 h, followed only by a gradual rise to ~0.25 V at extended times. In contrast, the PC-based electrolyte showed a slightly higher initial overpotential (~0.20 V) accompanied by temporal fluctuations, suggesting less homogeneous lithium deposition and a comparatively less stable SEI, though still maintaining compatibility over prolonged cycling. Beyond symmetric cell testing, the BC-based SPE delivered almost full practical specific capacity of about 150 mAh g^{-1} at low C-rate at RT, showcasing viable practical application in solid lithium metal batteries.

Overall, in this work, we presented an energy-efficient route for producing high-performance transparent SPEs by integrating UV-crosslinking, polymer blending, and cyclic carbonate additives, thereby promising RT next-generation SSLMBs. Particularly, the combination of stable cycling, high CE, and satisfactory rate performance further confirmed the robustness of BC as a functional plasticizer in UV-cured PEO–PEC polymer electrolytes.

CRediT authorship contribution statement

Rijul Bajaj: Writing – original draft, Validation, Methodology, Investigation, Data curation. **Hamideh Darjazi:** Writing – review & editing, Validation, Supervision, Methodology, Investigation. **Matteo Gastaldi:** Methodology. **Leonardo Balducci:** Validation, Methodology, Investigation, Data curation. **Giuseppe Antonio Elia:** Writing – review & editing, Validation, Methodology. **Claudio Gerbaldi:** Writing – review & editing, Validation, Supervision, Funding acquisition.

Declaration of competing interest

The authors declare that they have no known competing financial interests or personal relationships that could have appeared to influence the work reported in this paper.

Acknowledgements

The PSIONIC project has received funding from the European Commission Horizon Europe Research and Innovation Programme under Grant Agreement N. 101069703. Support by the European Union's Horizon Europe research and innovation program under the Marie Skłodowska-Curie Actions (RIDERS Doctoral Network, Grant Agreement N. 101120432, https://www.riders-dn.eu) is also acknowledged. Part of this study was carried out within the "Enabling high-energy, room temperature all solid-state lithium metal batteries with advanced polymer-based electrolytes and high-voltage cathodes through enhanced interface control (EnabLi)" project, funded by the Ministero dell'Università e della Ricerca within the PRIN 2022 program (D.D. 104 - 02/02/2022). The manuscript reflects only the authors' views and opinions, neither the European Union nor the European Commission can be considered responsible for them. Support under the MUR program "Dipartimenti di Eccellenza 2023–2027" (CUP E17G22001490006) is gratefully acknowledged.

Appendix A. Supplementary data

Supplementary data to this article can be found online at https://doi.org/10.1016/j.jpowsour.2026.239777.

Data availability

Data will be made available on request.

References

[1] H. Darjazi, M. Falco, F. Colò, L. Balducci, G. Piana, F. Bella, G. Meligrana, F. Nobili, G.A. Elia, C. Gerbaldi, Electrolytes for Sodium Ion Batteries: The Current Transition from Liquid to Solid and Hybrid systems, Advanced Materials 36 (2024) 2313572. https://doi.org/10.1002/adma.202313572.

[2] Y.-C. Jung, M.-S. Park, D.-H. Kim, M. Ue, A. Eftekhari, D.-W. Kim, Room-Temperature performance of Poly(Ethylene Ether Carbonate)-Based solid polymer electrolytes for All-Solid-State lithium batteries, Scientific Reports 7 (2017) 17482. https://doi.org/10.1038/s41598-017-17697-0.

[3] S. Ferrari, M. Falco, A.B. Muñoz-García, M. Bonomo, S. Brutti, M. Pavone, C. Gerbaldi, Solid-State Post li metal ion Batteries: a sustainable forthcoming reality? Advanced Energy Materials 11 (2021) 2100785. https://doi.org/10.1002/aenm.202100785.

[4] S. Porporato, H. Darjazi, M. Gastaldi, A. Piovano, A. Perez, B. Yécora, A. Fina, G. Meligrana, G.A. Elia, C. Gerbaldi, On the Use of Recycled PVB to Develop Sustainable Separators for Greener Li-Ion Batteries, Advanced Sustainable Systems 9 (2024) 2400569. https://doi.org/10.1002/adsu.202400569.

[5] S. Zhao, Q. Wu, W. Ma, L. Yang, Polyethylene Oxide-Based Composites as Solid-State Polymer Electrolytes for lithium Metal Batteries: A mini review, Frontiers in Chemistry 8 (2020) 640. https://doi.org/10.3389/fchem.2020.00640.

[6] G. Rollo-Walker, N. Malic, X. Wang, J. Chiefari, M. Forsyth, Development and progression of polymer electrolytes for batteries: influence of structure and chemistry, Polymers 13 (2021) 4127. https://doi.org/10.3390/polym13234127.

[7] K. Pożyczka, M. Marzantowicz, J.R. Dygas, F. Krok, SYSTEM LITFSI, Electrochimica Acta 227 (2016) 127–135. https://doi.org/10.1016/j.electacta.2016.12.172.

[8] Y. Zhang, W. Feng, Y. Zhen, P. Zhao, X. Wang, L. Li, Effects of lithium salts on PEO-based solid polymer electrolytes and their all-solid-state lithium-ion batteries, Ionics 28 (2022) 2751–2758. https://doi.org/10.1007/s11581-022-04525-3.

[9] D.K. Pradhan, B.K. Samantaray, R.N.P. Choudhary, A.K. Thakur, Effect of plasticizer on structure—property relationship in composite polymer electrolytes, Journal of Power Sources 139 (2004) 384–393. https://doi.org/10.1016/j.jpowsour.2004.05.050.

[10] X. Andrieu, J.F. Fauvarque, A. Goux, T. Hamaide, R. M'hamdi, T. Vicedo, Solid polymer electrolytes based on statistical poly (ethylene oxide-propylene oxide) copolymers, Electrochimica Acta 40 (1995) 2295–2299. https://doi.org/10.1016/0013-4686(95)00181-d.

[11] N. Molinari, J.P. Mailoa, B. Kozinsky, Effect of salt concentration on ion clustering and transport in polymer solid electrolytes: A Molecular dynamics study of PEO–LITFSI, Chemistry of Materials 30 (2018) 6298–6306. https://doi.org/10.1021/acs.chemmater.8b01955.

[12] K.-S. Ji, H.-S. Moon, J.-W. Kim, J.-W. Park, Role of functional nano-sized inorganic fillers in poly(ethylene) oxide-based polymer electrolytes, Journal of Power Sources 117 (2003) 124–130. https://doi.org/10.1016/s0378-7753(03)00159-9.

[13] M. Falco, C. Simari, C. Ferrara, J.R. Nair, G. Meligrana, F. Bella, I. Nicotera, P. Mustarelli, M. Winter, C. Gerbaldi, Understanding the effect of UV-Induced Cross-Linking on the physicochemical properties of highly performing PEO/LITFSI-Based polymer electrolytes, Langmuir 35 (2019) 8210–8219. https://doi.org/10.1021/acs.langmuir.9b00041.

[14] R. Arunkumar, R.S. Babu, M.U. Rani, S. Rajendran, Influence of plasticizer on ionic conductivity of PVC-PBMA polymer electrolytes, Ionics 23 (2017) 3097–3109. https://doi.org/10.1007/s11581-017-2101-2.

[15] A.M. Kirchberger, P. Walke, J. Venturini, L. Van Wüllen, T. Nilges, Highly conductive PEO/PAN-Based SN-Containing electrospun membranes as solid polymer electrolytes, Membranes 15 (2025) 196. https://doi.org/10.3390/membranes15070196.

[16] S. Mohapatra, S. Sharma, A. Sriperumbuduru, S.R. Varanasi, S. Mogurampelly, Effect of succinonitrile on ion transport in PEO-based lithium-ion battery electrolytes, The Journal of Chemical Physics 156 (2022) 214903. https://doi.org/10.1063/5.0087824.

[17] L. Herbers, V. Küpers, M. Winter, P. Bieker, An ionic liquid- and PEO-based ternary polymer electrolyte for lithium metal batteries: an advanced processing solvent-free approach for solid electrolyte processing, RSC Advances 13 (2023) 17947–17958. https://doi.org/10.1039/d3ra02488a.

[18] J.B. Haskins, W.R. Bennett, J.J. Wu, D.M. Hernández, O. Borodin, J.D. Monk, C. W. Bauschlicher, J.W. Lawson, Computational and Experimental Investigation of Li-Doped Ionic Liquid Electrolytes: [pyr14][TFSI], [pyr13][FSI], and [EMIM][BF4], The Journal of Physical Chemistry B 118 (2014) 11295–11309. https://doi.org/10.1021/jp5061705.

[19] T. Melin, R. Lundström, E.J. Berg, Revisiting the Ethylene Carbonate–Propylene Carbonate Mystery with Operando Characterization, Advanced Materials Interfaces 9 (2021) 2101258. https://doi.org/10.1002/admi.202101258.

[20] R. Lundström, N. Gogoi, T. Melin, E.J. Berg, Unveiling reaction pathways of ethylene carbonate and vinylene carbonate in Li-Ion batteries, The Journal of Physical Chemistry C 128 (2024) 8147–8153. https://doi.org/10.1021/acs.jpcc.4c00927.

[21] X. You, M. Chaudhari, S. Rempe, L.R. Pratt, Dielectric properties of ethylene carbonate and propylene carbonate using molecular dynamics simulations, ECS Transactions 69 (2015) 107–111. https://doi.org/10.1149/06901.0107ecst.

[22] R. Payne, I.E. Theodorou, Dielectric properties and relaxation in ethylene carbonate and propylene carbonate, The Journal of Physical Chemistry 76 (1972) 2892–2900. https://doi.org/10.1021/j100664a019.

[23] L.R.A.K. Bandara, M.A.K.L. Dissanayake, B. -e. Mellander, Ionic conductivity of plasticized(PEO)-$LiCF_3SO_3$ electrolytes, Electrochimica Acta 43 (1998) 1447–1451. https://doi.org/10.1016/s0013-4686(97)10082-2.

[24] T. Fujinaga, K. Izutsu, Propylene carbonate: purification and tests for purity, Pure and Applied Chemistry 27 (1971) 273–280. https://doi.org/10.1351/pac197127010273.

[25] S. Das, A. Ghosh, Ionic conductivity and dielectric permittivity of PEO-$LiClO_4$ solid polymer electrolyte plasticized with propylene carbonate, AIP Advances 5 (2015) 027125. https://doi.org/10.1063/1.4913320.

[26] P. Wang, X. Sun, Y. An, X. Zhang, C. Yuan, S. Zheng, K. Wang, Y. Ma, Additives to propylene carbonate-based electrolytes for lithium-ion capacitors, Rare Metals 41 (2022) 1304–1313. https://doi.org/10.1007/s12598-021-01887-x.

[27] D.M. Seo, D. Chalasani, B.S. Parimalam, R. Kadam, M. Nie, B.L. Lucht, Reduction reactions of carbonate solvents for lithium ion batteries, ECS Electrochemistry Letters 3 (2014) A91–A93. https://doi.org/10.1149/2.0021409eel.

[28] S. Moharana, G. West, A.S. Menon, W.L. Da Silva, M. Walker, M.J. Loveridge, Combined Stabilizing of the Solid–Electrolyte Interphase with Suppression of Graphite Exfoliation via Additive-Solvent Optimization in Li-Ion Batteries, ACS Applied Materials & Interfaces 15 (2023) 50185–50195. https://doi.org/10.1021/acsami.3c10792.

[29] K. Chiba, T. Ueda, Y. Yamaguchi, Y. Oki, F. Saiki, K. Naoi, Electrolyte systems for high withstand voltage and durability II. Alkylated cyclic carbonates for electric Double-Layer capacitors, Journal of the Electrochemical Society 158 (2011) A1320. https://doi.org/10.1149/2.038112jes.

[30] S.A. Suthanthiraraj, M.K. Vadivel, Effect of propylene carbonate as a plasticizer on $(PEO)_{50}AgCF_3SO_3$:SnO_2 nanocomposite polymer electrolyte, Applied Nanoscience 2 (2012) 239–246. https://doi.org/10.1007/s13204-012-0099-3.

[31] J. Kumełan, D. Tuma, S.P. Verevkin, G. Maurer, Solubility of hydrogen in the cyclic alkylene ester 1,2-butylene carbonate, Journal of Chemical & Engineering Data 53 (2008) 2844–2850. https://doi.org/10.1021/je800583r.

[32] K. Hayamizu, Y. Aihara, S. Arai, C.G. Martinez, Pulse-Gradient Spin-Echo ^1H, ^7Li, and ^{19}F NMR diffusion and ionic conductivity measurements of 14 organic electrolytes containing $LiN(SO_2CF_3)_2$, The Journal of Physical Chemistry B 103 (1999) 519–524. https://doi.org/10.1021/jp9825664.

[33] L.H. Hess, A. Balducci, 1,2-butylene carbonate as solvent for EDLCs, Electrochimica Acta 281 (2018) 437–444. https://doi.org/10.1016/j.electacta.2018.05.168.

[34] Y. Huang, L. Qi, H. Wang, Intercalation of anions into graphite electrode from butylene carbonate in activated carbon/graphite hybrid capacitors, Electrochimica Acta 258 (2017) 380–387. https://doi.org/10.1016/j.electacta.2017.11.066.

[35] I.L. Johansson, D. Brandell, J. Mindemark, Mechanically stable UV-Crosslinked Polyester-Polycarbonate solid polymer electrolyte for High-Temperature batteries, Batteries & Supercaps 3 (2020) 527–533. https://doi.org/10.1002/batt.201900228.

[36] L. Balducci, H. Darjazi, A. Piovano, G.A. Elia, C. Gerbaldi, On the role of UV crosslinking to enhance moderate-temperature operation of truly solid-state Li-metal batteries based on recycled-PVB-modified polyether electrolytes, Journal of Power Sources 662 (2025) 238704. https://doi.org/10.1016/j.jpowsour.2025.238704.

[37] A. Patriarchi, H. Darjazi, M. Barcaioni, L. Minnetti, A. Fina, A. Filippov, F.U. Shah, O.N. Antzutkin, M.Á. Muñoz-Márquez, F. Nobili, Sustainable solid-state polymer electrolyte based on PEO-Xanthan gum blend for enhanced lithium-metal batteries, Journal of Power Sources 663 (2025) 238856. https://doi.org/10.1016/j.jpowsour.2025.238856.

[38] F. Gambino, M. Gastaldi, A. Jouhara, S. Malburet, S. Galliano, N. Cavallini, G. Colucci, M. Zanetti, A. Fina, G.A. Elia, C. Gerbaldi, Formulating PEO-polycarbonate blends as solid polymer electrolytes by solvent-free extrusion, Journal of Power Sources Advances 30 (2024) 100160. https://doi.org/10.1016/j.powera.2024.100160.

[39] Z. Li, R. Mogensen, J. Mindemark, T. Bowden, D. Brandell, Y. Tominaga, Ion-Conductive and Thermal Properties of a Synergistic Poly(ethylene carbonate)/Poly(trimethylene carbonate) Blend Electrolyte, Macromolecular Rapid Communications 39 (2018) 1800146. https://doi.org/10.1002/marc.201800146.

[40] J. Mindemark, M.J. Lacey, T. Bowden, D. Brandell, Beyond PEO—Alternative host materials for Li^+ -conducting solid polymer electrolytes, Progress in Polymer Science 81 (2018) 114–143. https://doi.org/10.1016/j.progpolymsci.2017.12.004.

[41] M. Vilkman, V. Pechancová, S. Mousavi, M. Mosallaei, D. Paul, F. Obrezkov, Extrusion coating as a tool for sustainable solid-state battery manufacturing, Zenodo (CERN European Organization for Nuclear Research) (2024). https://doi.org/10.5281/zenodo.14056673.

[42] Z. Qiu, L. Miao, W. Yang, Crystallization and melting behavior of biodegradable poly(butylene succinate-co-butylene carbonate), Journal of Polymer Science Part B Polymer Physics 44 (2006) 1556–1561. https://doi.org/10.1002/polb.20816.

[43] K. Platen, F. Langer, J. Schwenzel, Influence of screw design and process parameters on the product quality of PEO:LITFSI solid electrolytes using Solvent-Free melt extrusion, Batteries 10 (2024) 183. https://doi.org/10.3390/batteries10060183.

[44] J. Evans, C.A. Vincent, P.G. Bruce, Electrochemical measurement of transference numbers in polymer electrolytes, Polymer 28 (1987) 2324–2328. https://doi.org/10.1016/0032-3861(87)90394-6.

[45] M. Marzantowicz, J.R. Dygas, F. Krok, A. Łasińska, Z. Florjańczyk, E. Zygadło-Monikowska, A. Affek, Crystallization and melting of PEO:LiTFSI polymer electrolytes investigated simultaneously by impedance spectroscopy and polarizing microscopy, Electrochimica Acta 50 (2005) 3969–3977. https://doi.org/10.1016/j.electacta.2005.02.053.

[46] M. Navarra, L. Lombardo, P. Bruni, L. Morelli, A. Tsurumaki, S. Panero, F. Croce, Gel Polymer Electrolytes Based on Silica-Added Poly(ethylene oxide) Electrospun Membranes for Lithium Batteries, Membranes 8 (2018) 126. https://doi.org/10.3390/membranes8040126.

[47] O. Guchok, G. Ardel, T.D. Keidar, H. Nakar, H. Ragones, D. Kaplan, A. Zheng, S. Greenbaum, I. Lounev, A. Greenbaum, Y. Feldman, D. Golodnitsky, Understanding of the ion transport in blended TPU-PEO polymer electrolytes, Journal of Solid State Electrochemistry (2025). https://doi.org/10.1007/s10008-025-06323-z.

[48] M. Gastaldi, F. Gambino, H. Darjazi, A. Jouhara, S. Malburet, M. Zanetti, G. Saracco, G.A. Elia, C. Gerbaldi, Dry extrusion of poly(ethylene oxide)-polycarbonate all-solid-state electrolytes for Li-metal batteries: effect of UV-crosslinking on the electrochemical performance, Materials Today Energy 52 (2025) 101947. https://doi.org/10.1016/j.mtener.2025.101947.

[49] H.M.J.C. Pitawala, M.A.K.L. Dissanayake, V.A. Seneviratne, B.-E. Mellander, I. Albinson, Effect of plasticizers (EC or PC) on the ionic conductivity and thermal properties of the $(PEO)_9LiTf$: Al_2O_3 nanocomposite polymer electrolyte system, Journal of Solid State Electrochemistry 12 (2008) 783–789. https://doi.org/10.1007/s10008-008-0505-7.

[50] R. Pathak, K. Chen, A. Gurung, K.M. Reza, B. Bahrami, J. Pokharel, A. Baniya, W. He, F. Wu, Y. Zhou, K. Xu, Q. Qiao, Fluorinated hybrid solid-electrolyte-

interphase for dendrite-free lithium deposition, Nature Communications 11 (2020) 93. https://doi.org/10.1038/s41467-019-13774-2.
[51] X. Li, Z. Li, C. Li, F. Tian, Z. Qiao, D. Lei, C. Wang, Facilitating uniform lithium-ion transport via polymer-assisted formation of unique interfaces to achieve a stable 4.7 V Li metal battery, National Science Review 12 (2025) nwaf182. https://doi.org/10.1093/nsr/nwaf182.
[52] S. Menkin, J.B. Fritzke, R. Larner, C. De Leeuw, Y. Choi, A.B. Gunnarsdóttir, C. P. Grey, Insights into soft short circuit-based degradation of lithium metal batteries, Faraday Discussions 248 (2023) 277–297. https://doi.org/10.1039/d3fd00101f.
[53] E.B. Springl, D. Sarkar, M. Mühlau, V.K. Michaelis, T. Nilges, Performance optimization of Electrospun Lithium-Ion conducting PAN/PEO solid polymer electrolyte, Inorganic Chemistry 64 (2025) 19752–19763. https://doi.org/10.1021/acs.inorgchem.5c03238.
[54] X. Liu, Q. Liang, L. Chen, J. Tang, J. Liu, M. Tang, Z. Wang, PEO-Based Solid-State electrolytes reinforced by high strength, interconnected MOF networks, ACS Applied Energy Materials 6 (2023) 4881–4891. https://doi.org/10.1021/acsaem.3c00371.
[55] Z. Geng, Y. Huang, G. Sun, R. Chen, W. Cao, J. Zheng, H. Li, In-situ polymerized solid-state electrolytes with stable cycling for Li/LiCoO2 batteries, Nano Energy 91 (2021) 106679. https://doi.org/10.1016/j.nanoen.2021.106679.
[56] C. Xin, K. Wen, S. Guan, C. Xue, X. Wu, L. Li, C.-W. Nan, A Cross-Linked Poly (Ethylene Oxide)-Based electrolyte for All-Solid-State lithium metal batteries with long cycling stability, Frontiers in Materials 9 (2022) 864478. https://doi.org/10.3389/fmats.2022.864478.
[57] D. Mankovsky, D. Lepage, M. Lachal, L. Caradant, D. Aymé-Perrot, M. Dollé, Water content in solid polymer electrolytes: the lost knowledge, Chemical Communications 56 (2020) 10167–10170. https://doi.org/10.1039/d0cc03556d.
[58] N.A. Ramlee, Y. Tominaga, Preparation and characterization of poly(ethylene carbonate)/poly(lactic acid) blends, Journal of Polymer Research 25 (2018) 54. https://doi.org/10.1007/s10965-018-1451-4.
[59] H. Beyer, S. Meini, N. Tsiouvaras, M. Piana, H.A. Gasteiger, Thermal and electrochemical decomposition of lithium peroxide in non-catalyzed carbon cathodes for Li–air batteries, Physical Chemistry Chemical Physics 15 (2013) 11025. https://doi.org/10.1039/c3cp51056e.
[60] Z. Xue, D. He, X. Xie, Poly(ethylene oxide)-based electrolytes for lithium-ion batteries, Journal of Materials Chemistry A 3 (2015) 19218–19253. https://doi.org/10.1039/c5ta03471j.
[61] K. Platen, F. Langer, R. Bayer, R. Hollmann, J. Schwenzel, M. Busse, Influence of Molecular Weight and Lithium Bis(trifluoromethanesulfonyl)imide on the Thermal Processability of Poly(ethylene oxide) for Solid-State Electrolytes, Polymers 15 (2023) 3375. https://doi.org/10.3390/polym15163375.
[62] M. Zhang, F. Makhlooghiazad, U. Pal, M. Maleki, S. Kondou, G.A. Elia, C. Gerbaldi, M. Forsyth, Synergistic Combination of Cross-Linked Polymer and Concentrated Ionic Liquid for Electrolytes with High Stability in Solid-State Lithium Metal Batteries, ACS Applied Polymer Materials 6 (2024) 14469–14476. https://doi.org/10.1021/acsapm.4c02520.
[63] Y. Zou, Y. He, H. Li, S. Deng, W. Tang, S. Deng, PEO-based electrolyte filled with UV-cured 3D cross-linked polymer network for lithium metal batteries, Journal of Energy Storage 104 (2024) 114619. https://doi.org/10.1016/j.est.2024.114619.
[64] R. Fong, A. Robertson, P. Mallon, R. Thompson, The Impact of Plasticizer and Degree of Hydrolysis on Free Volume of Poly(vinyl alcohol) Films, Polymers 10 (2018) 1036. https://doi.org/10.3390/polym10091036.
[65] C.Y. Son, Z.-G. Wang, Ion transport in small-molecule and polymer electrolytes, The Journal of Chemical Physics 153 (2020) 100903. https://doi.org/10.1063/5.0016163.
[66] J. Pan, A.P. Charnay, W. Zheng, M.D. Fayer, Revealing lithium ion transport mechanisms and solvation structures in carbonate electrolytes, Journal of the American Chemical Society 146 (2024) 35329–35338. https://doi.org/10.1021/jacs.4c13423.
[67] H. Jiang, Q. Zhang, Y. Zhang, L. Sui, G. Wu, K. Yuan, X. Yang, Li-Ion solvation in propylene carbonate electrolytes determined by molecular rotational measurements, Physical Chemistry Chemical Physics 21 (2019) 10417–10422. https://doi.org/10.1039/c8cp07552b.
[68] Y.-Q. Wang, H. Xu, B. Cao, J. Ma, Z.-W. Yu, In situ species analysis of a Lithium-Ion battery electrolyte containing LiTFSI and propylene carbonate, The Journal of Physical Chemistry Letters 15 (2024) 5047–5055. https://doi.org/10.1021/acs.jpclett.4c00641.
[69] M.P. Rosenwinkel, R. Andersson, J. Mindemark, M. Schönhoff, Coordination effects in polymer electrolytes: fast Li^+ transport by weak ion binding, The Journal of Physical Chemistry C 124 (2020) 23588–23596. https://doi.org/10.1021/acs.jpcc.0c08369.
[70] Q. Qian, Y. Yang, H. Shao, Solid electrolyte interphase formation by propylene carbonate reduction for lithium anode, Physical Chemistry Chemical Physics 19 (2017) 28772–28780. https://doi.org/10.1039/c7cp04839d.